Electronic Supplementary Material (ESI) for Physical Chemistry Chemical Physics.

Supporting Information

Core Structure Dependence of Cycloreversion Dynamics in Diarylethene Analogs

Chana R. Honick, Garvin M. Peters, Jamie D. Young, John D. Tovar, and Arthur E. Bragg*
Department of Chemistry, Johns Hopkins University
3400 N. Charles St., Baltimore, MD 21218
**artbragg@jhu.edu*

1. Synthetic details for **2**
2. Determination of molar absorptivities for open and closed isomers
3. Global fitting results for ultrafast transient absorption data and examples of temperature-dependent transient data
4. Determination of cycloreversion quantum yields: method and results
5. Calculation of competitive excited-state deactivation rates and thermodynamic activation parameters.
6. Spectrum of UV hand-lamp emission.

1. Synthetic Details for 2:

2-methyl-3-((4-(methylthio)thiophen-3-yl)ethynyl)benzo[b]thiophene

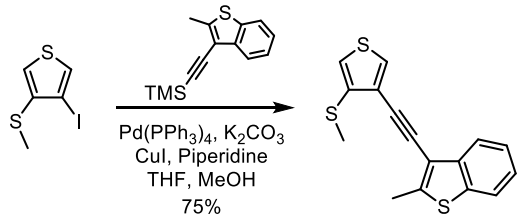

A solution of 3-iodo-4-(methylthio)thiophene (1.00 g, 3.90 mmol), trimethyl((2-methylbenzo[b]thiophen-3-yl)ethynyl)silane (954 mg, 3.90 mmol), and potassium carbonate (1.19 g, 8.58 mmol) in THF (70 mL) was sparged with N_2 for 15 min. Under positive N_2 pressure, copper(I) iodide (37 mg, 0.54 mmol) and $Pd(PPh_3)_4$ (225 mg, 0.540 mmol) were added, followed by piperidine (3.85 mL, 39.0 mmol) and methanol (30 mL). The reaction mixture was refluxed for 18 h, after which it was washed twice with sat. NH_4Cl (25 mL) and once with brine (50 mL). The organic layer was dried over anhydrous $MgSO_4$, filtered, and concentrated under reduced pressure. The off-white solid was purified by column chromatography (silica, 80:20 hexanes:dichloromethane) to yield a white solid (819 mg, 2.73 mmol, 70%). ^{1}H NMR (400 MHz, $CDCl_3$): δ 7.96 (d, 1H), 7.73 (d, 1H), 7.59 (d, 1H), 7.41 (t, 1H), 7.32 (t, 1H), 6.91 (d, 1H), 2.75 (s, 3H), 2.55 (s, 1H). ^{13}C (^{1}H) NMR (100 MHz, $CDCl_3$): δ 145.4, 140.0, 137.6, 136.9, 129.1, 124.9, 124.6, 123.2, 122.7, 122.1, 118.4, 115.8, 87.7, 86.0, 17.0, 15.6. HRMS (EI) found m/z = 300.0091 (M^+), calculated for $C_{16}H_{12}S_3$: 300.0101.

3-(3-iodothieno[3,4-b]thiophen-2-yl)-2-methylbenzo[b]thiophene

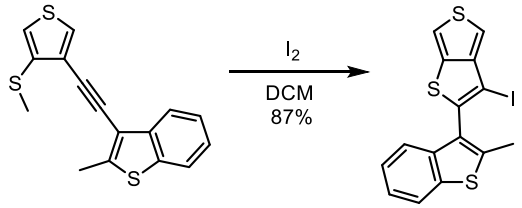

A Solution of 2-methyl-3-((4-(methylthio)thiophen-3-yl)ethynyl)benzo[b]thiophene (665 mg, 2.21 mmol) in dichloromethane (50 mL) was titrated with an iodine solution (674 mg, 2.66 mmol in 100 mL DCM) at room temperature until the starting material was consumed, as monitored by TLC. The reaction mixture was then washed once with sat. $Na_2S_2O_3$ (10 mL), twice with DI H_2O (10 mL), and once with brine (10 mL). The organic layer was dried over anhydrous $MgSO_4$, filtered, and concentrated under reduced pressure. The yellow solid was purified by column chromatography (silica, 80:20 hexanes:dichloromethane) to yield a white solid (794 mg, 1.92 mmol, 87%). ^{1}H NMR (400 MHz, $CDCl_3$): δ 7.80 (m, 1H), 7.52 (m, 1H), 7.44 (d, 1H), 7.40 (d, 1H), 7.32 (m, 2H), 2.54 (s, 3H). ^{13}C (^{1}H) NMR (100 MHz, $CDCl_3$): δ 150.4, 141.8, 141.6, 139.3, 138.1, 137.1, 127.1, 124.6, 124.4, 122.8, 122.2, 115.1, 112.4, 74.0, 15.4. HRMS (EI) found m/z = 411.8901 (M^+), calculated for $C_{15}H_9IS_3$: 411.8911.

3,3'-(thieno[3,4-b]thiophene-2,3-diyl)bis(2-methylbenzo[b]thiophene) TT-BT

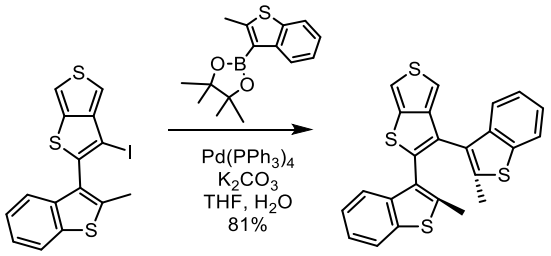

$Pd(PPh_3)_4$ (111 mg, 9.6×10^{-5} mol), 4,4,5,5-tetramethyl-2-(2-methylbenzo[b]thiophen-3-yl)-1,3,2-dioxaborolane (578 mg, 2.11 mmol), and 3-(3-iodothieno[3,4-b]thiophen-2-yl)-2-methylbenzo[b]thiophene (790 mg, 1.92 mmol) were added to a 25 mL Schlenk flask, which was evacuated and backfilled with N_2 three times. THF (10 mL), and saturated K_2CO_3 solution (5 mL) was added, and the reaction mixture was heated to reflux for 16 h. The mixture was then diluted with diethyl ether (20 mL) and washed twice with water (30 mL) and once with brine (30 mL). The organic layer was dried over anhydrous $MgSO_4$, filtered, and concentrated under reduced pressure. The brown solid was purified by column chromatography (silica, 80:20 hexanes:DCM) to yield the product as a white solid (669 mg, 1.55 mmol, 81%). ^{1}H NMR (400 MHz, $CDCl_3$): δ 7.96 (d, 1H), 7.73 (m, 1H), 7.59 (m, 2H), 7.32 (m, 4H), 7.06 (m, 2H).

2. Determination of molar absorptivities for open and closed isomers:

Molar absorptivities of open and closed isomers were determined using a multi-step method. The steps and results for each photoswitch are outlined below.

(1) **Determination of molar absorptivity for open switches:** Several solutions of pure open switch were prepared at various known concentrations. UV-Vis spectra were collected for these solutions in a 1-mm cuvette (Figure S1). Beer's Law plots (absorption vs. concentration) were prepared for each switch (Figure S1). The molar absorptivity for the pure open switch at a specific reference wavelength in the UV (**1c**: 260nm, **2c**: 250nm, **3c**: 250nm, **4c**: 290nm, **5c**: 250nm) was obtained from the slope of each plot. A summary of these molar absorptivities is listed below in Table S1.

(2) **Measurement of the pure/isolated cyclized absorption spectrum:** The absorption spectrum of the pure closed form was determined using HPLC to separate the closed and open isomers as described in the paper.

(3) **Determination of molar absorptivity for the closed isomer:** Solutions of pure open isomer was prepared for each photoswitch and irradiated at 325 nm for a period of time using a handheld lamp. A UV-Vis spectrum was taken of each sample periodically to track the increase in closed population in the mixture. The spectra of the pure closed photoswitch, as determined with HPLC separation, was scaled to match the absorption intensity of the visible absorption band appearing upon irradiation (top panels, Figures S2-S6). The former was then subtracted from the latter to isolate the amount of absorption due to remaining pure open species alone (middle panels, Figures S2-S6). Once the spectra for the pure open species were isolated, the concentrations associated with each spectrum were determined using the molar absorptivity of the open isomer. The change in concentration of open isomer with irradiation time was taken as the concentration for the closed isomer for a Beer's Law analysis to determine the molar absorptivity for the closed species at specific wavelengths (**1c**: 530nm, **2c**: 500nm, **3c**: 530nm, **4c**: 590nm, **5c**: 530nm); see bottom panels of Figures S2-S6. A list of these molar absorptivities is listed in Table S1. The UV-Vis spectra obtained from each closed isomer via HPLC separation was scaled accordingly to obtain wavelength-dependent absorptivity shown in Figure 1.

Table S1. Molar absorptivities at specific wavelengths for **1c-5c** in open and cyclized form.

Species	Open		Cyclized	
	λ (nm)	ε (M^{-1} cm^{-1} /10^4)	λ (nm)	ε (M^{-1} cm^{-1} /10^4)
1	260	1.5	530	0.73
2	250	2.7	500	0.74
3	250	2.1	530	0.53
4	290	4.5	590	1.1
5	250	2.2	530	0.54

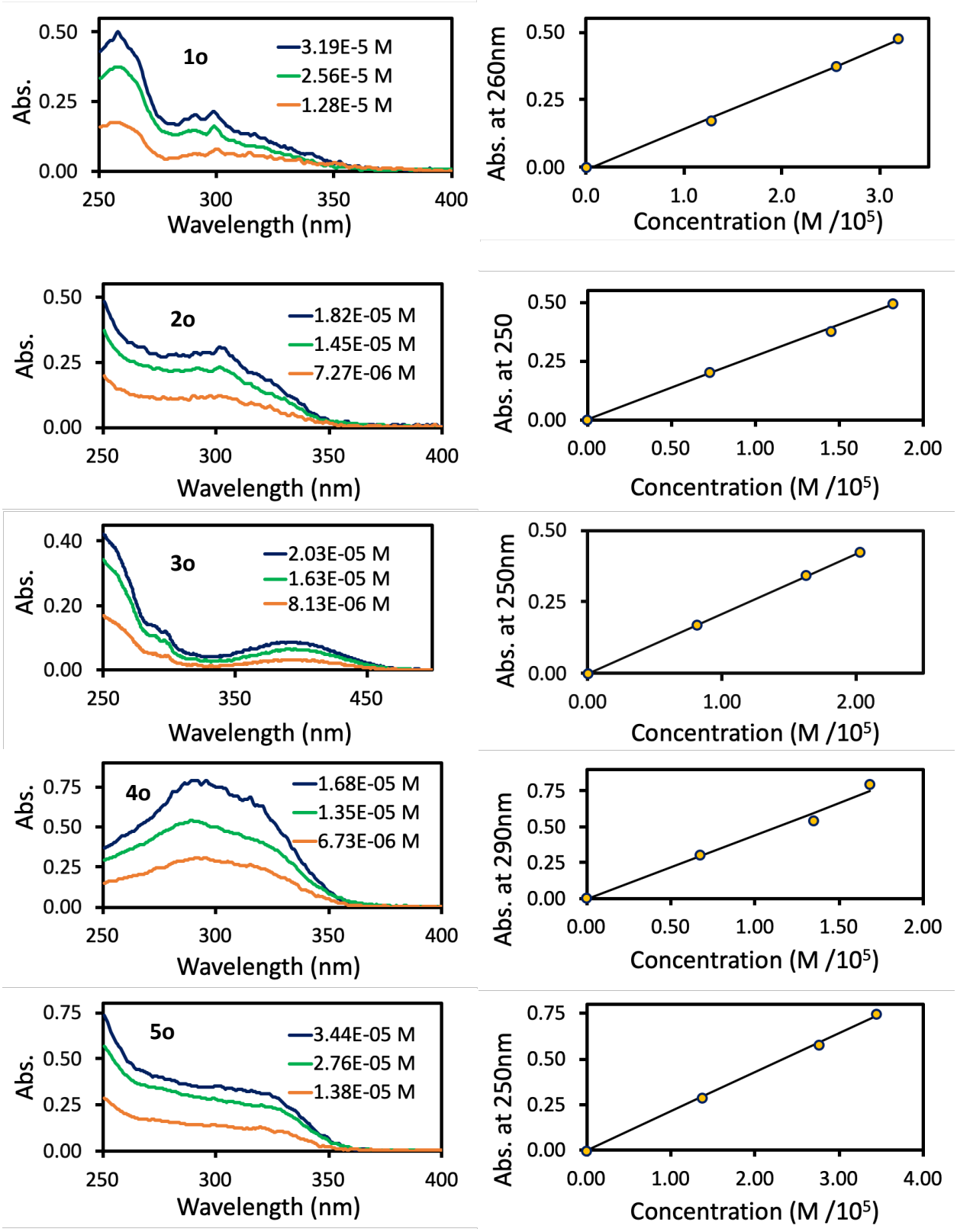

Figure S1. UV-Vis spectra for **1o-5o** at various concentrations (left) and corresponding Beer's Law plots (right). The latter were prepared at the following peak absorption wavelengths; **1o**: 260nm, **2o**: 250nm, **3o**: 250nm, **4o**: 290nm, **5o**: 250nm.

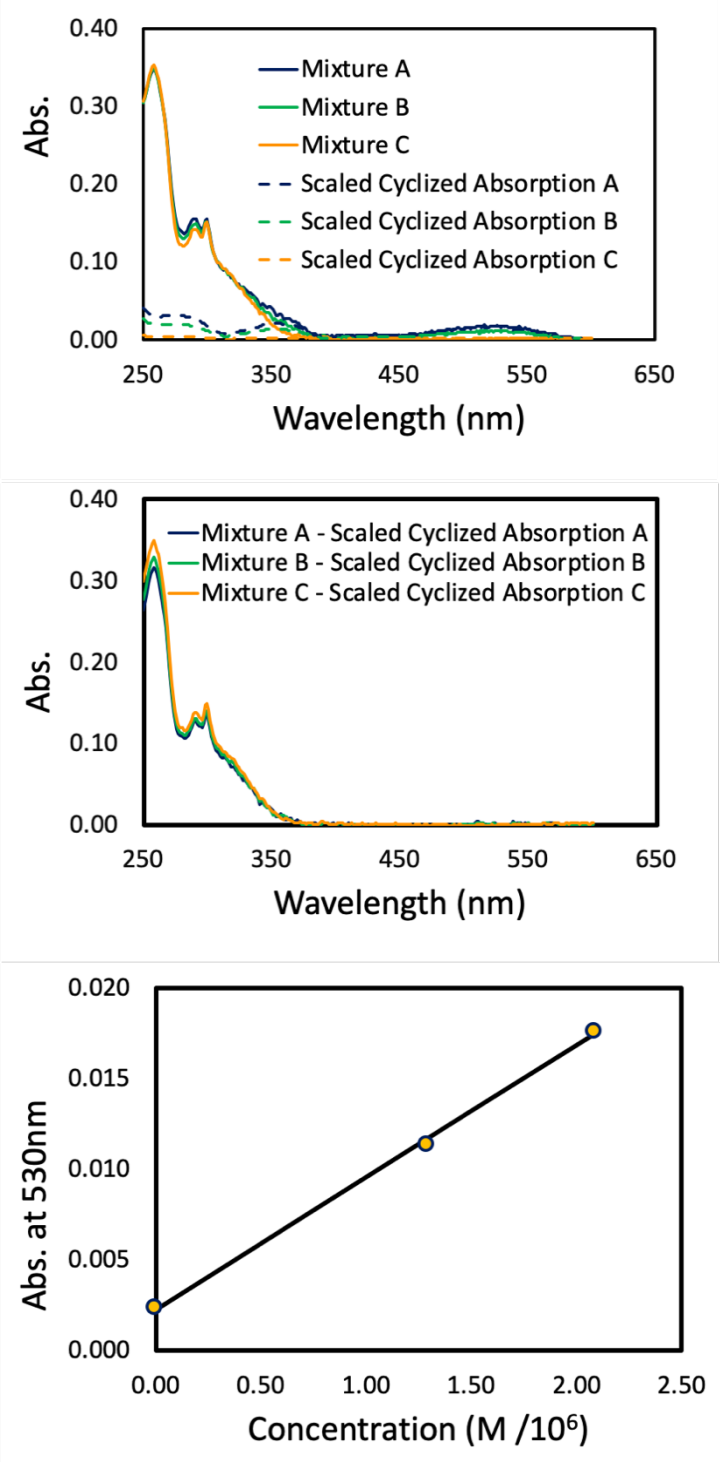

Figure S2. Steps for determining the molar absorptivity for **1c**: UV-Vis spectra of photochemical mixtures plotted with the scaled **1c** absorption spectrum determined using HPLC separation (top); difference of spectra in top panel to isolate contribution from (and therefore change in concentration of) open isomer (middle); Beer's Law plot for closed species (bottom).

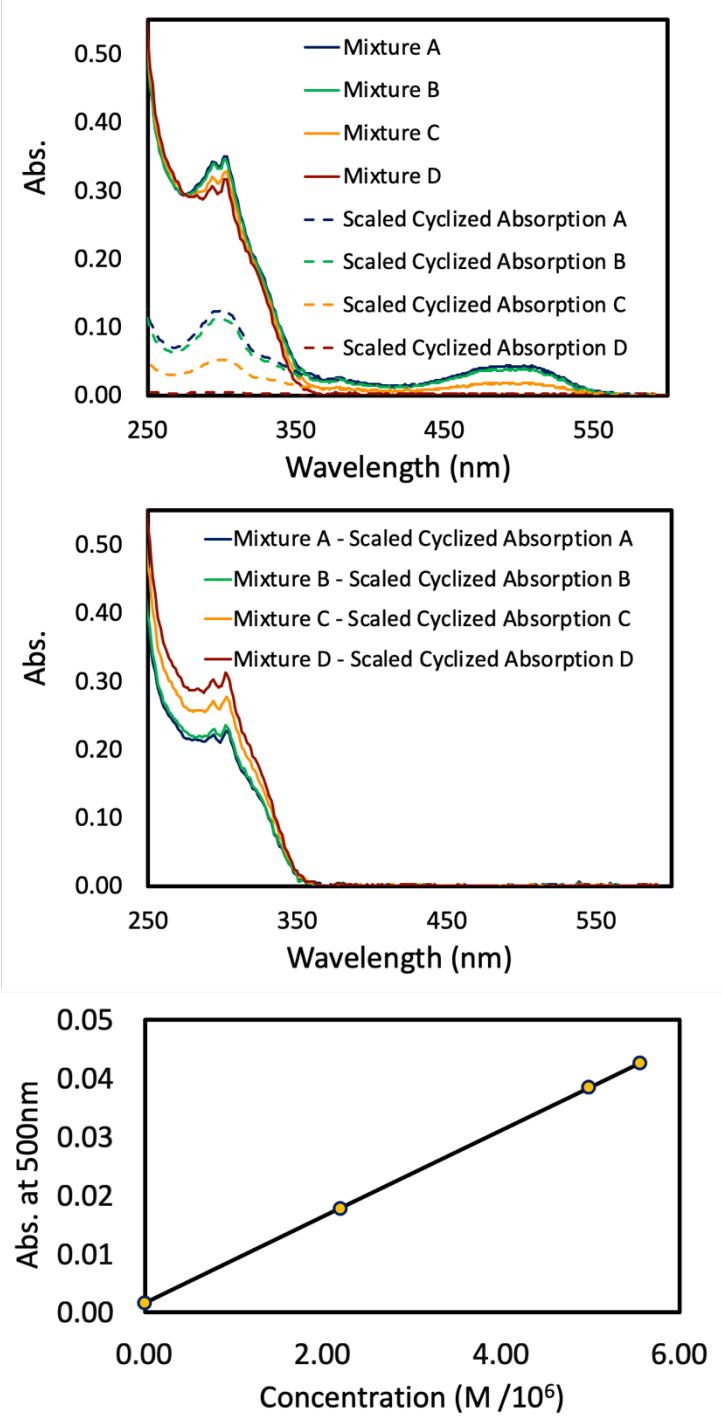

Figure S3. Steps for determining the molar absorptivity for **2c**: UV-Vis spectra of photochemical mixtures plotted with the scaled **2c** absorption spectrum determined using HPLC separation (top); difference of spectra in top panel to isolate contribution from (and therefore change in concentration of) open isomer (middle); Beer's Law plot for closed species (bottom).

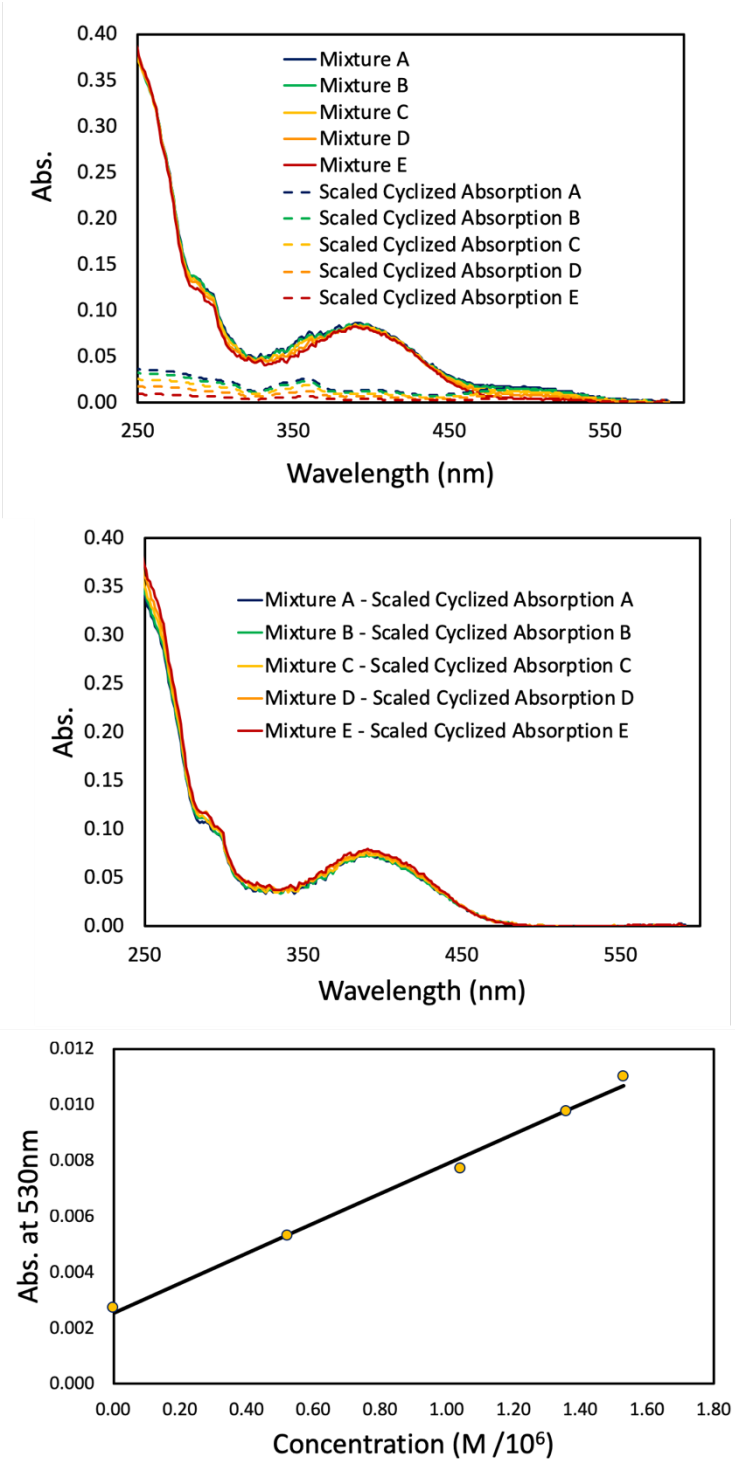

Figure S4. Steps for determining the molar absorptivity for **3c**: UV-Vis spectra of photochemical mixtures plotted with the scaled **3c** absorption spectrum determined using HPLC separation (top); difference of spectra in top panel to isolate contribution from (and therefore change in concentration of) open isomer (middle); Beer's Law plot for closed species (bottom).

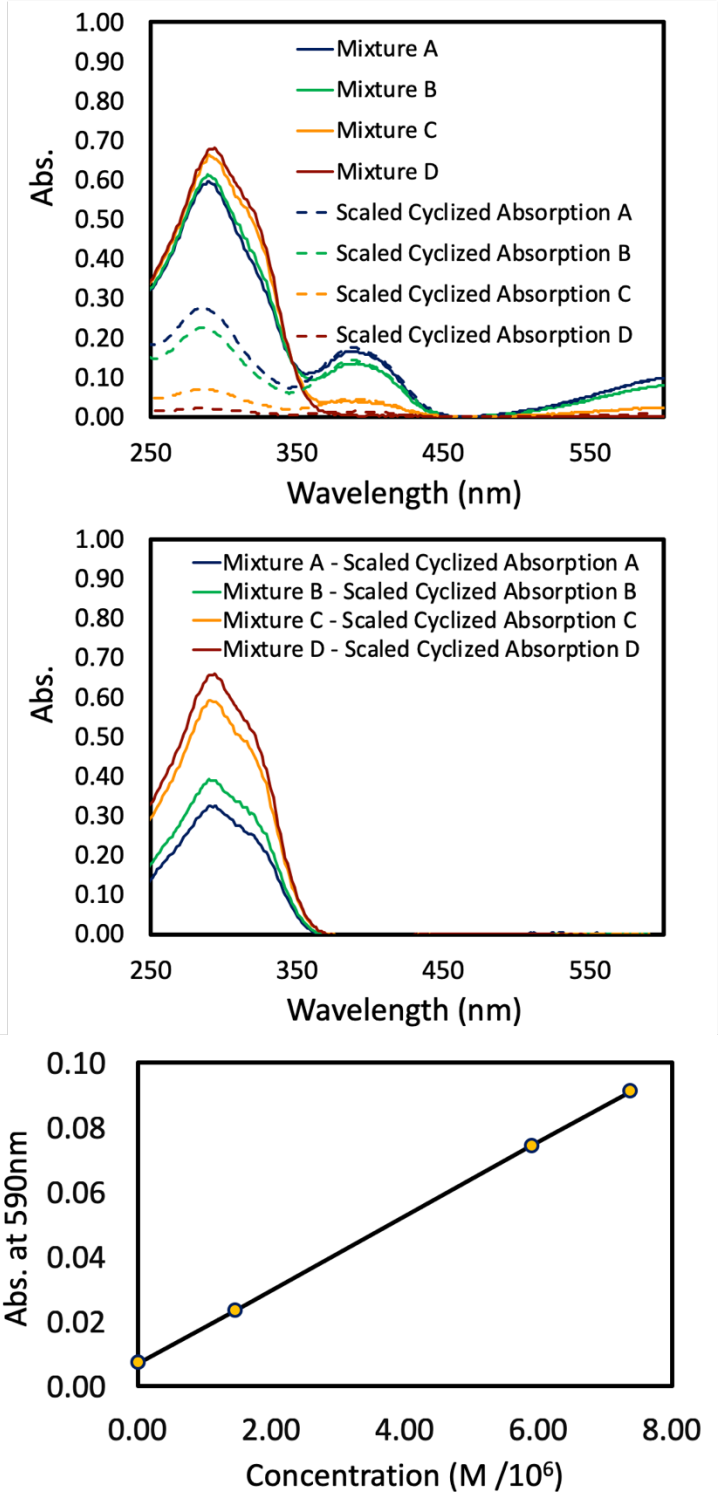

Figure S5. Steps for determining the molar absorptivity for **4c**: UV-Vis spectra of photochemical mixtures plotted with the scaled **4c** absorption spectrum determined using HPLC separation (top); difference of spectra in top panel to isolate contribution from (and therefore change in concentration of) open isomer (middle); Beer's Law plot for closed species (bottom).

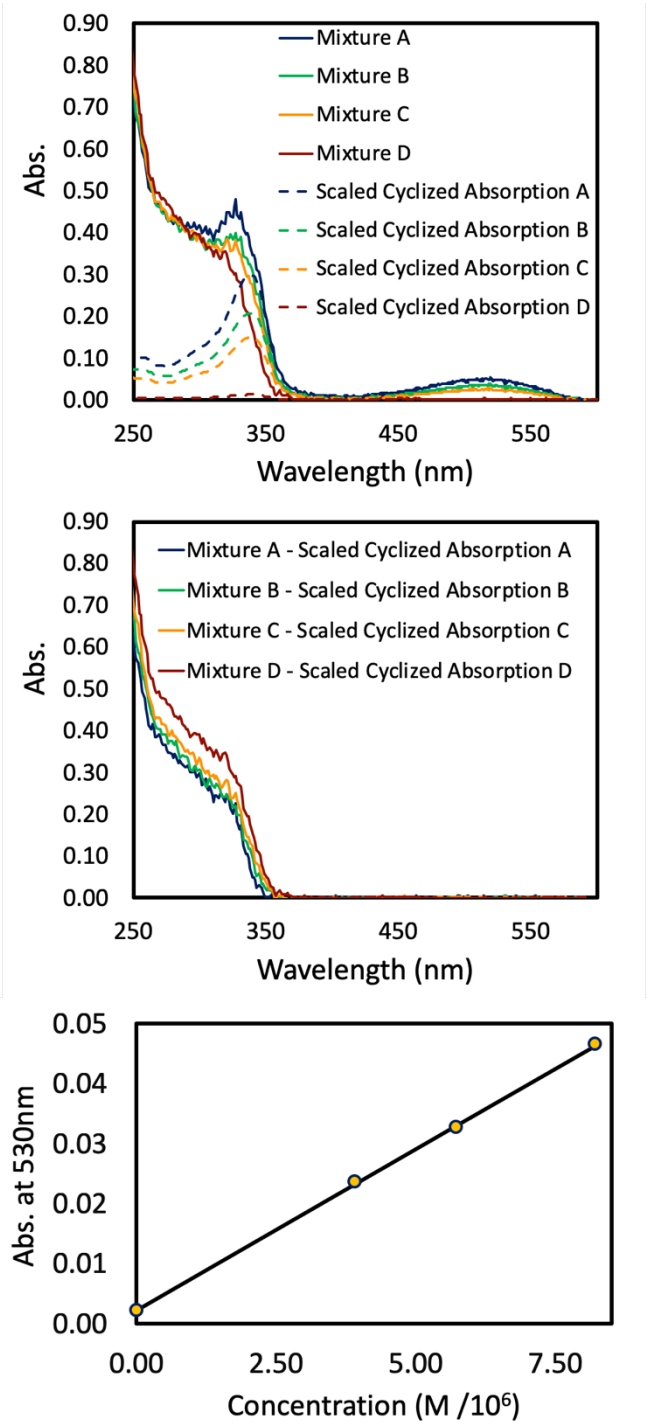

Figure S6. Steps for determining the molar absorptivity for **5c**: UV-Vis spectra of photochemical mixtures plotted with the scaled **5c** absorption spectrum determined using HPLC separation (top); difference of spectra in top panel to isolate contribution from (and therefore change in concentration of) open isomer (middle); Beer's Law plot for closed species (bottom).

3. Global fitting results for ultrafast transient absorption data:*

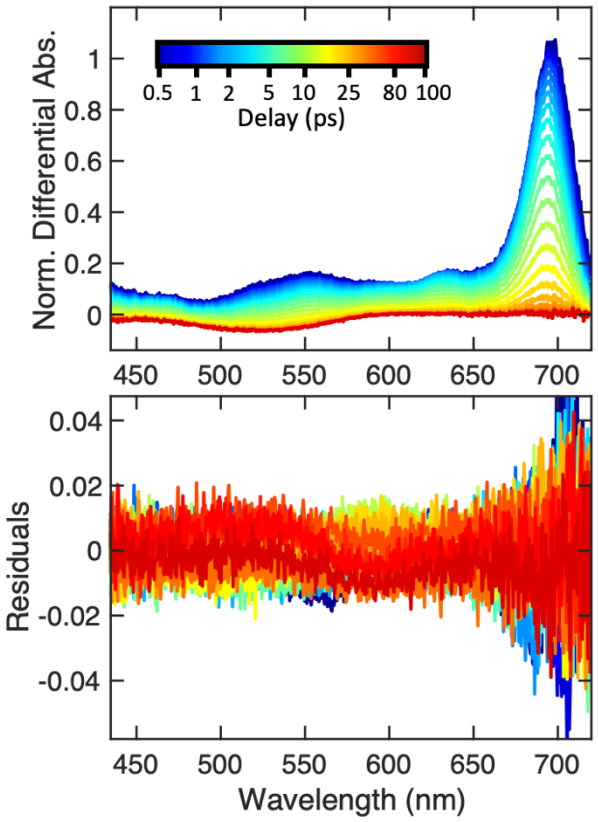

Figure S7. Spectral reconstruction from global fit (top) and residuals (bottom) for TA data collected with **1c** in acetonitrile. Data was normalized to intensity at 694 nm at 1 ps.

* All lifetimes are reported in the main text Table 1 and Table 2.

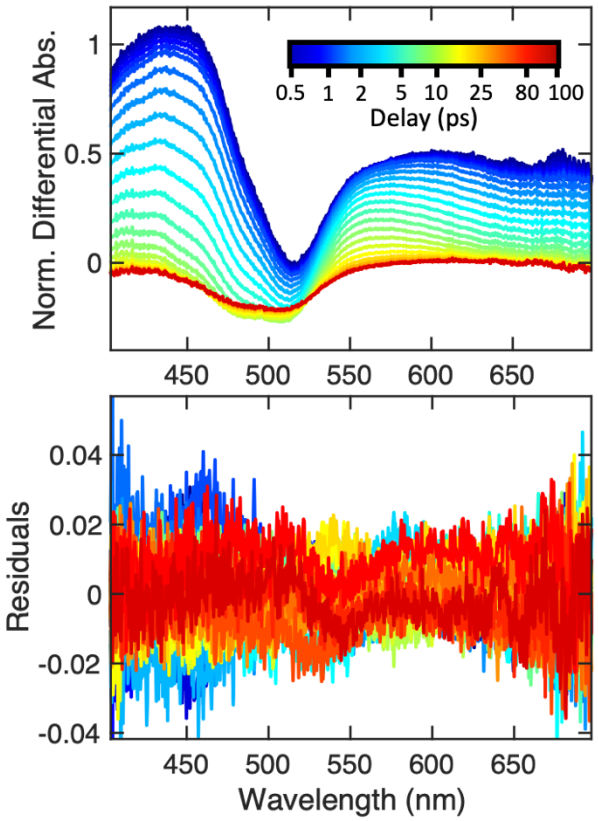

Figure S8. Spectral reconstruction from global fit (top) and residuals plot (bottom) for TA data collected with **2c** in acetonitrile. Data was normalized to intensity at 437 nm at 1 ps.

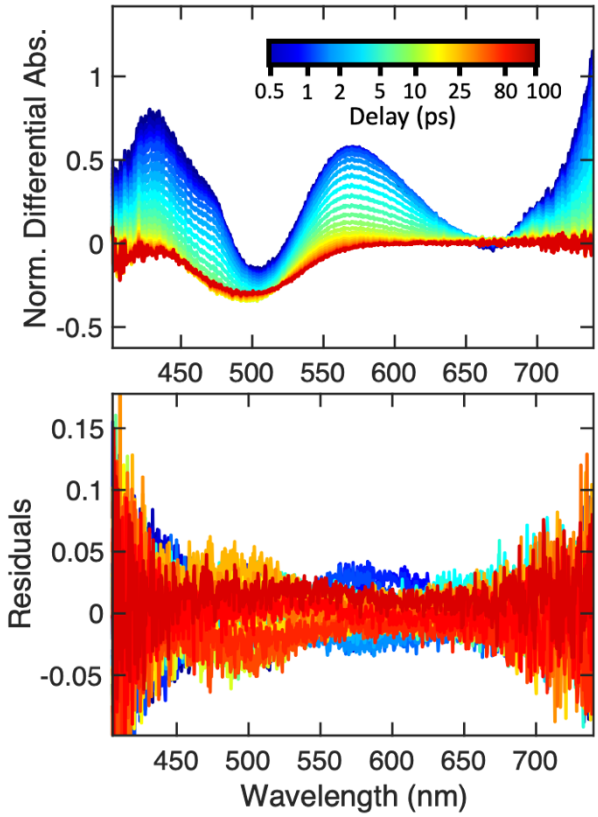

Figure S9. Spectral reconstruction from global fit (top) and residuals plot (bottom) for TA data collected with **3c** in acetonitrile. Data was normalized to intensity at 739 nm at 1 ps.

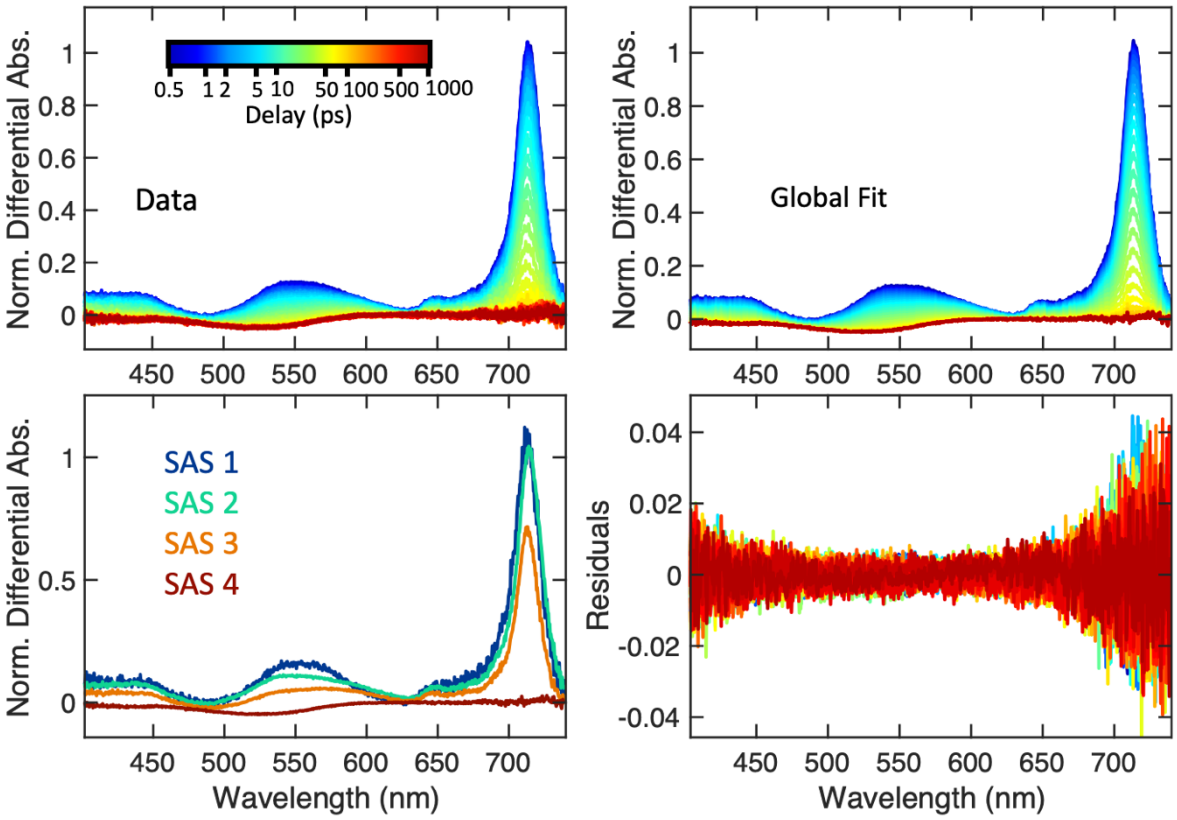

Figure S10. The transient absorption data (top, left), spectral reconstruction from global fit (top, right), species associated spectra (bottom, left) and residual plot (bottom, right) for **1c** in cyclohexane. Data was normalized to intensity at 714 nm at 1 ps.

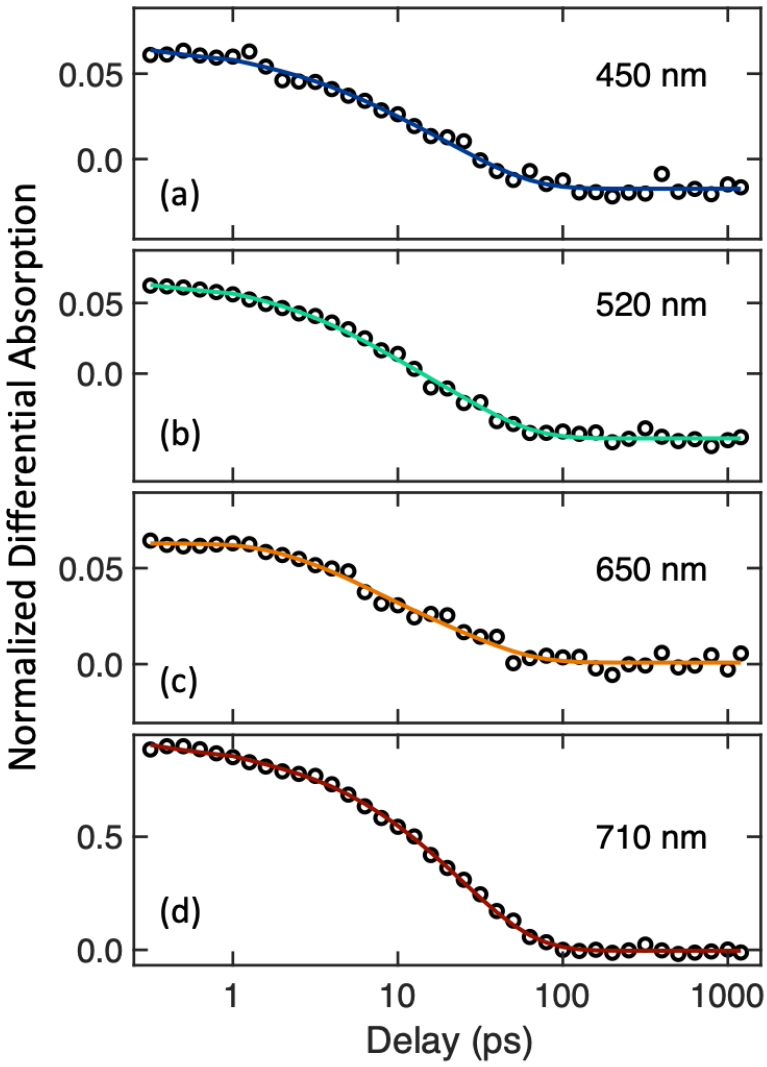

Figure S11. Time-dependent global fits for TA data collected with **1c** in cyclohexane (a-d). Data after 0.5 ps is plotted on a linear scale <1ps and on a logarithmic scale >1ps to clarify early time spectral dynamics.

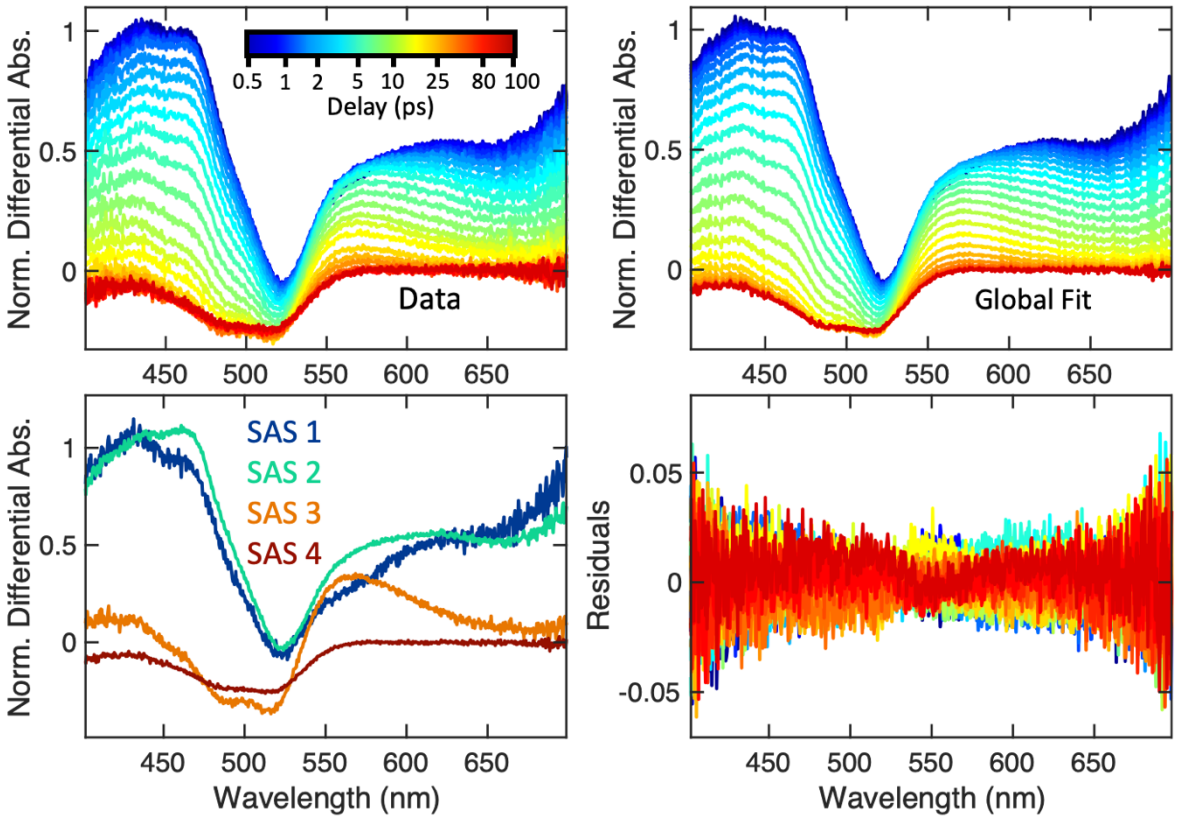

Figure S12. The transient absorption data (top, left), spectral reconstruction from global fit (top, right), species associated spectra (bottom, left) and residual plot (bottom, right) for **2c** in cyclohexane. Data was normalized to intensity at 438 nm at 1 ps.

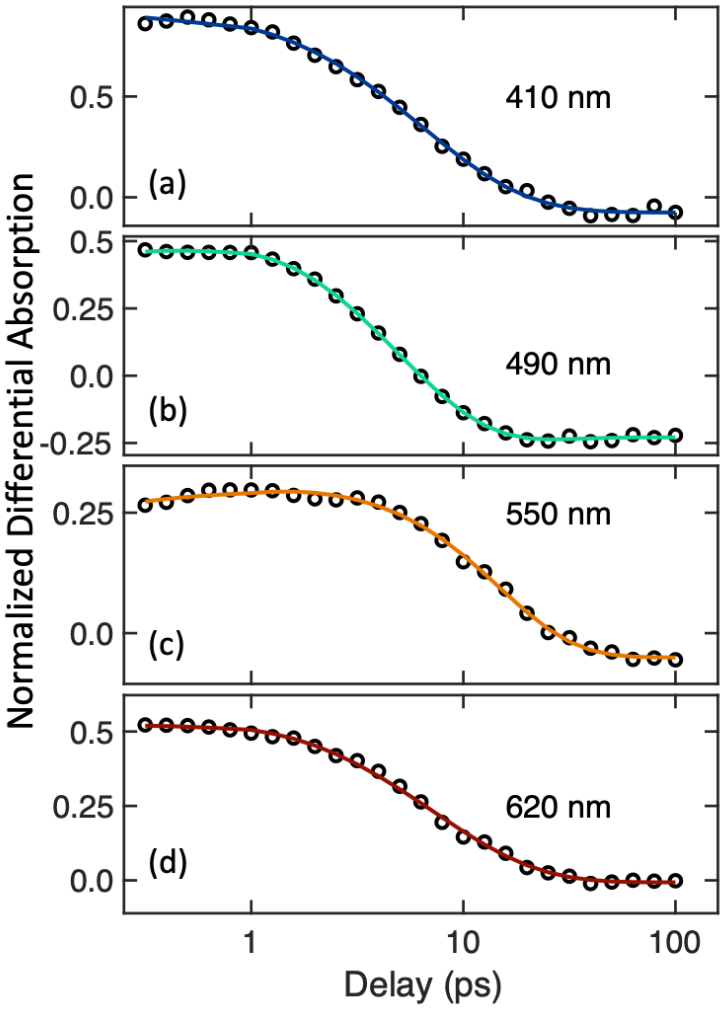

Figure S13. Time-dependent global fits for TA data collected with **2c** in cyclohexane (a-d). Data after 0.5 ps is plotted on a linear scale <1ps and on a logarithmic scale >1ps to clarify early time spectral dynamics.

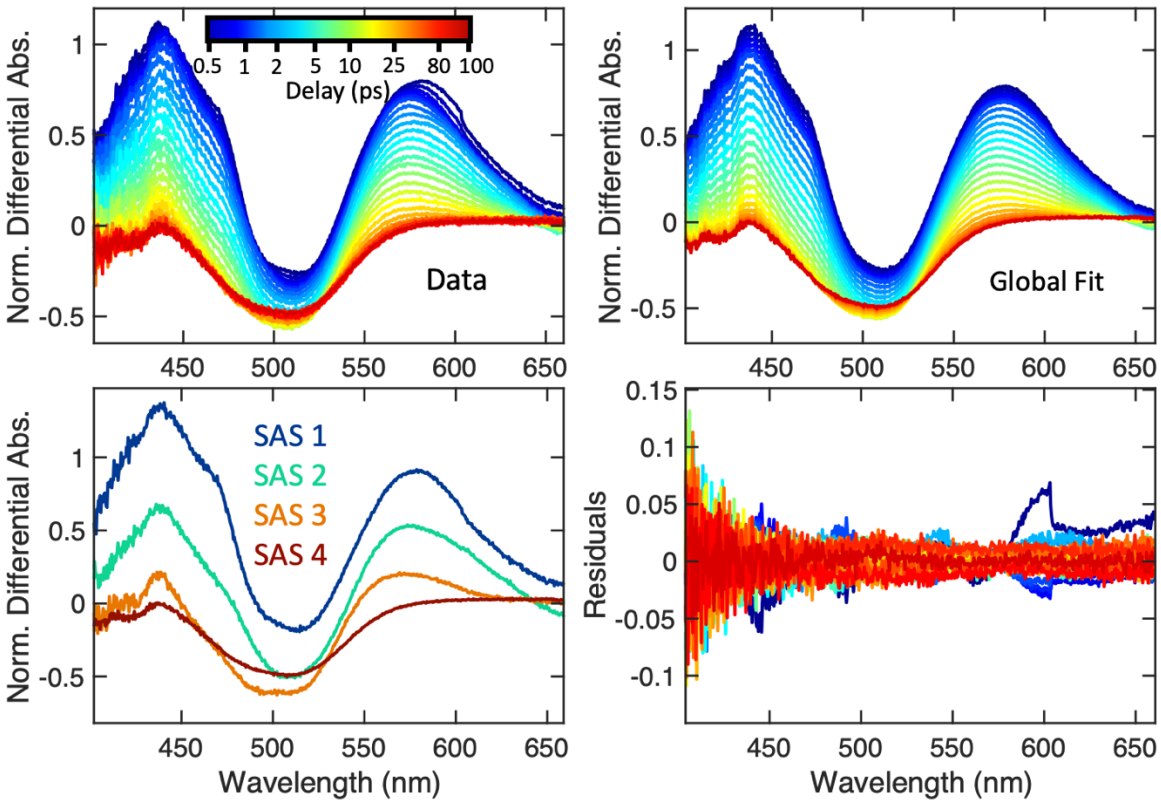

Figure S14. The transient absorption data (top, left), spectral reconstruction from global fit (top, right), species associated spectra (bottom, left) and residual plot (bottom, right) for **3c** in cyclohexane. Data was normalized to intensity at 436 nm 1 ps.

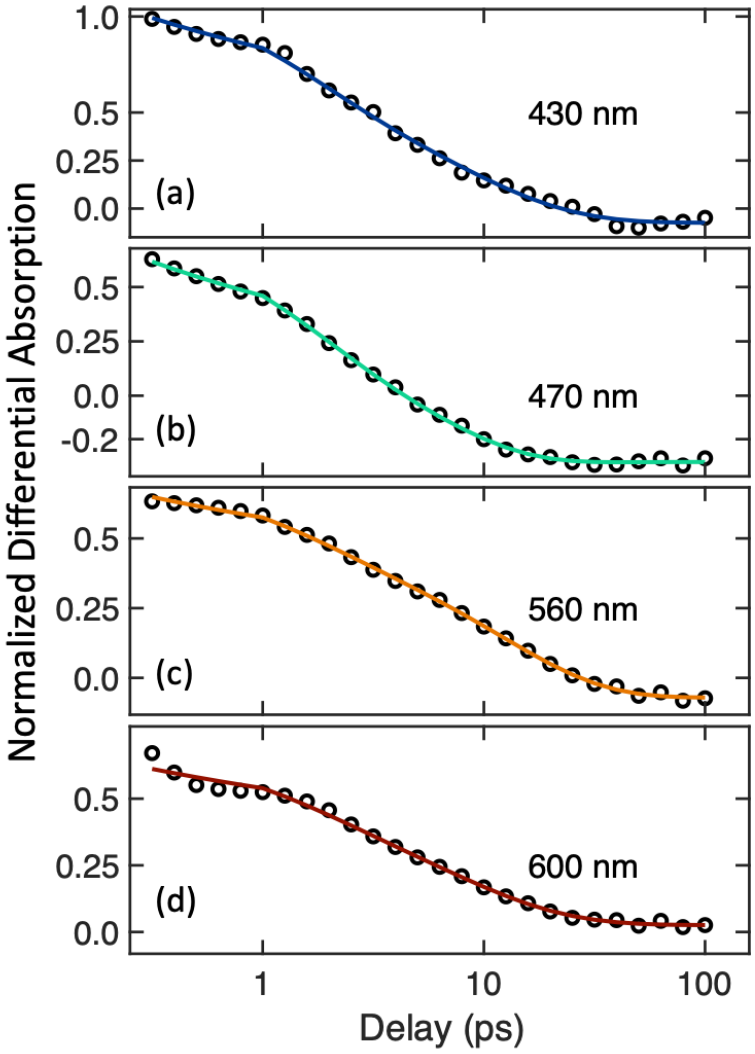

Figure S15. Time-dependent global fits for TA data collected with **3c** in cyclohexane (a-d). Data after 0.5 ps is plotted on a linear scale <1ps and on a logarithmic scale >1ps to clarify early time spectral dynamics.

The temperature dependent electronic lifetimes were determined by fitting a kinetic trace through each transient spectrum at a wavelength selective for excited-state absorption (i.e., away from regions where spectral signatures of vibrational cooling could be observed). Data was fit only after 1-1.5 ps to avoid fitting lifetimes for fast excited state spectral relaxation behaviors. Reference spectra were collected by setting the delay stage at a fixed delay so that the loss of intensity due purely to cycloreversion could be observed over the typical timescale for transient data acquisition. Experimental data was normalized by dividing the experimental trace by the reference trace. Representative traces for each switch at 298K are shown below.

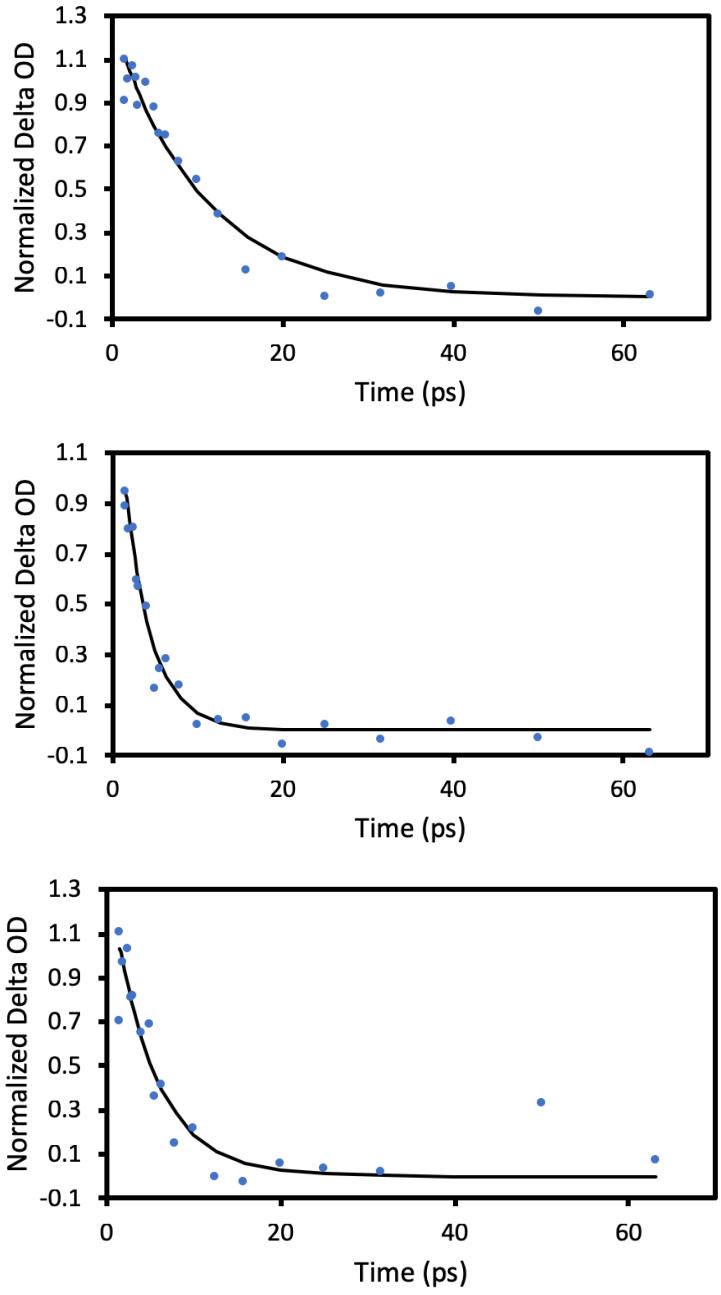

Figure S16. Decay traces for **1c** (top), **2c** (middle), and **3c** (bottom) at room temperature.

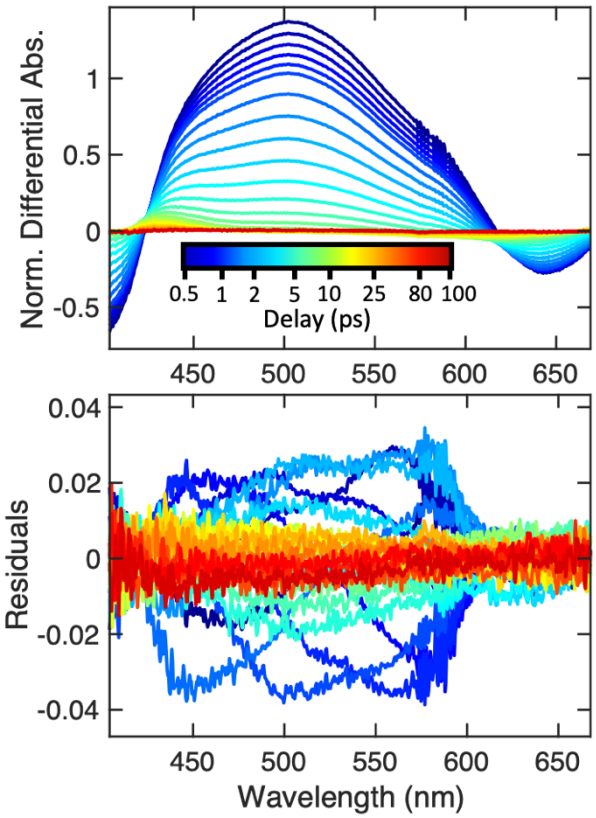

Figure S17. Spectral reconstruction from global fit (top) and residuals plot (bottom) for TA data collected with **4c** in acetonitrile. Data was normalized to intensity at 503 nm at 1 ps.

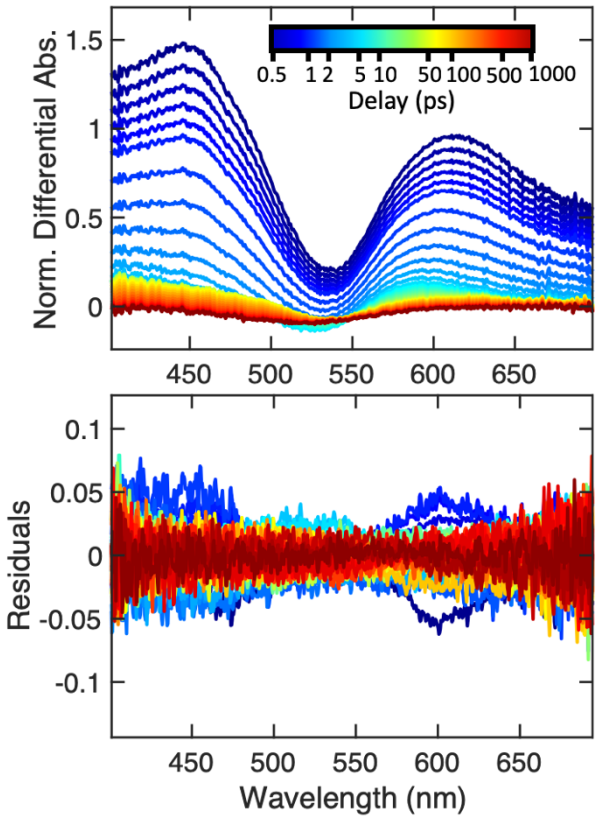

Figure S18. Spectral reconstruction from global fit (top) and residuals plot (bottom) for TA data collected with **5c** in acetonitrile. Data was normalized to intensity at 447 nm at 1 ps.

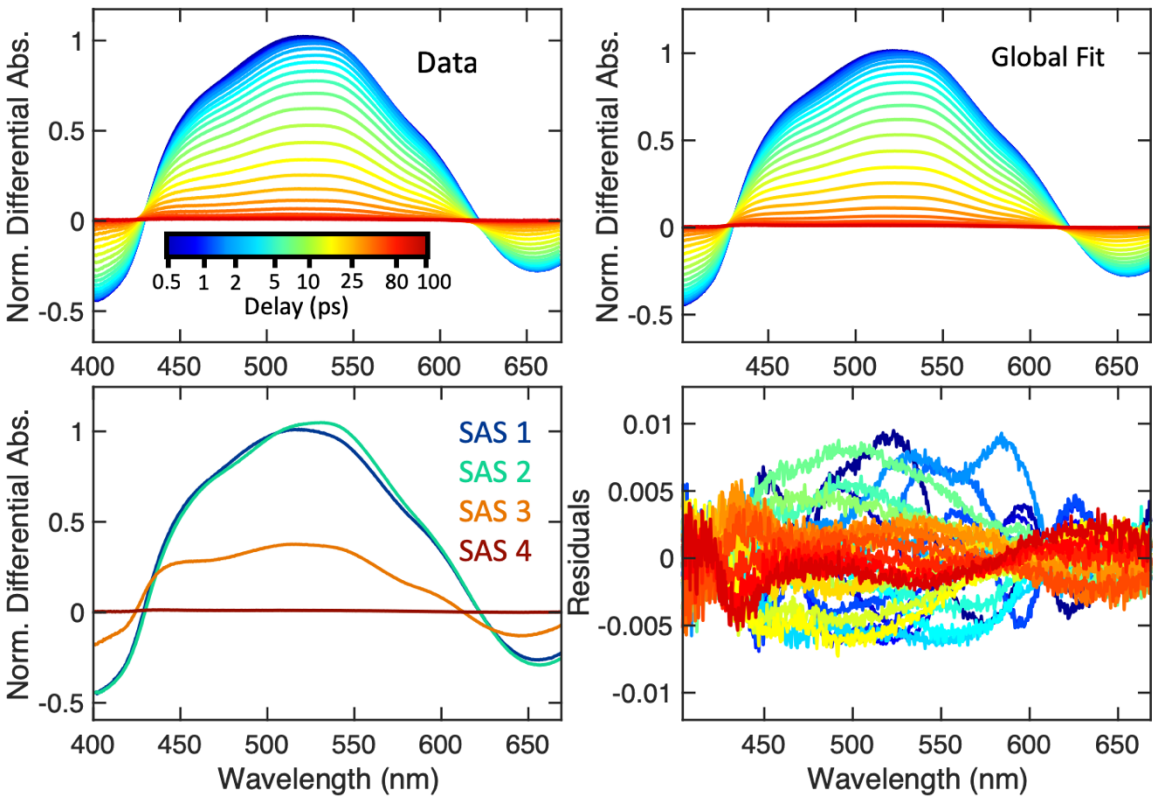

Figure S19. The transient absorption data (top, left), spectral reconstruction from global fit (top, right), species associated spectra (bottom, left) and residual plot (bottom, right) for **4c** in cyclohexane. Data was normalized to intensity at 526 nm at 1 ps.

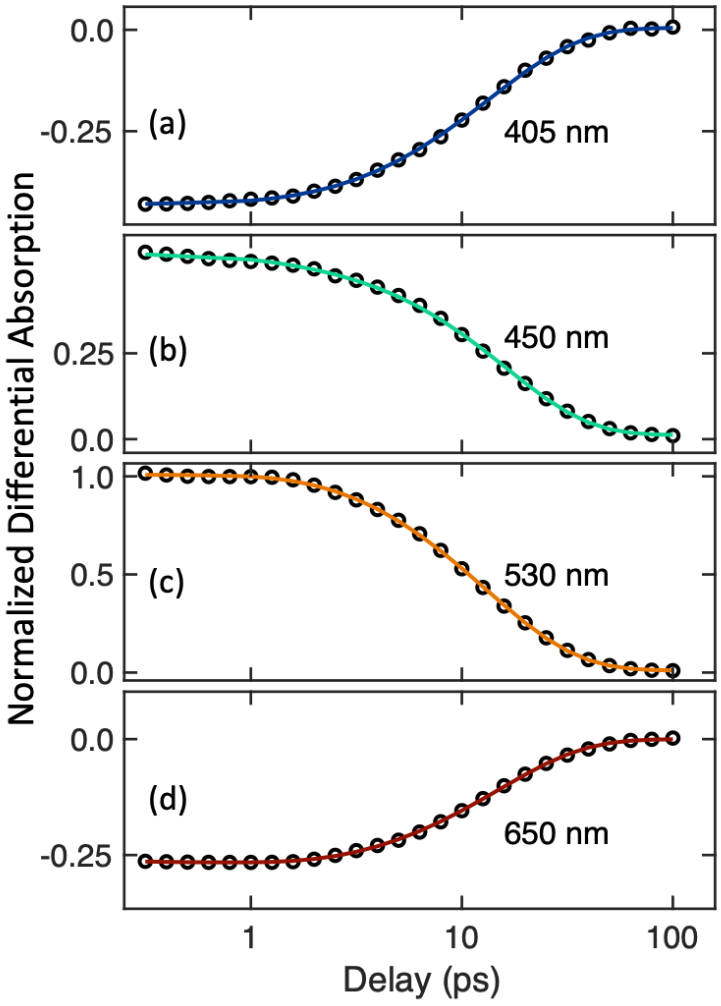

Figure S20. Time-dependent global fits for TA data collected with **4c** in cyclohexane (a-d). Data after 0.5 ps is plotted on a linear scale <1ps and on a logarithmic scale >1ps to clarify early time spectral dynamics.

4. Determination of cycloreversion quantum yields: method and results

Cycloreversion quantum yields were determined by actinometry as described in the methods section. The set-up for this involved LED irradiation of a stirred sample cuvette orthogonal to the beam direction of the UV-Vis light source through the sample. The absorbance at the irradiation wavelength was measured with time of irradiation. As only the closed isomer absorbs at visible wavelengths, the time-dependence of sample conversion could be modelled as:

$$\log\left(10^{A(t)}-1\right)-\log\left(10^{A(0)}-1\right)=-\frac{1000\varepsilon l n_p}{N_A v}\Phi_{CO}t \quad (1)$$

where ε is the molar absorptivity of the photoswitch, l is the pathlength of the cell, n_p is the photon flux, N_A is Avogadro's number, and v is the volume of the solution. This facilitates a linear fit of a function of absorbance with respect to time, with the slope that is the product of the quantum yield for cycloreversion, molar absorptivity at the irradiation wavelength, photon flux of the irradiation source and sample pathlength. Examples of linearized data for each switch and fits are presented in Figures S21-S25. Molar absorptivities were determined as described above. The photon flux was obtained by measuring the time-dependent conversion of a standard photoswitch with known quantum yield; a typical photon flux was $8.6\pm0.3\times10^{17}$ to $9.4\pm0.2\times10^{17}$ (for cyan LED) and $14.3\pm0.9\times10^{17}$ (for yellow LED).

In order to determine temperature-dependent quantum yields, changes in absorption intensity were recorded as a function of temperature to account for changes in molar absorptivity. In general, the absorbance was observed to increase slightly with decreasing temperature (Figure S26 and Table S3). Temperature dependent quantum yields are summarized in Table S4.

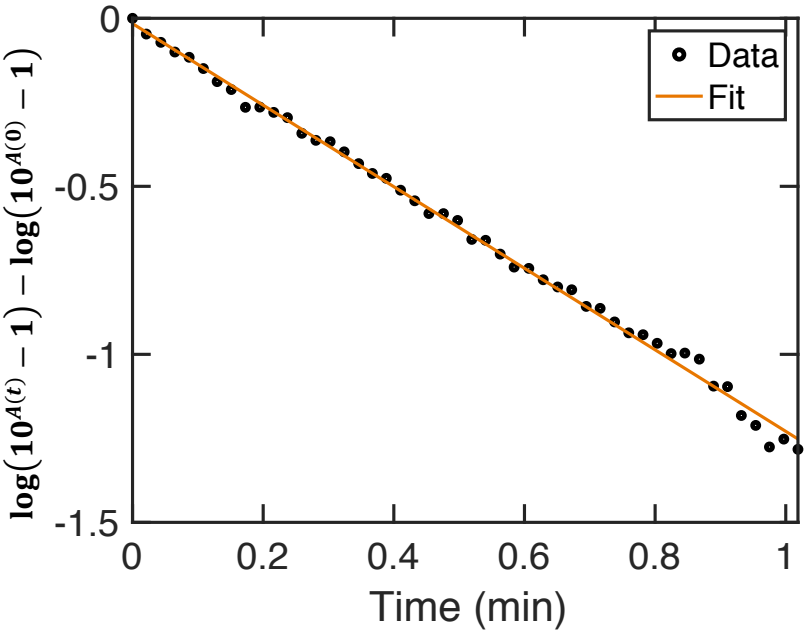

Figure S21. Linearized function of absorption vs. time used to determine the cycloreversion quantum yield of **1c**.

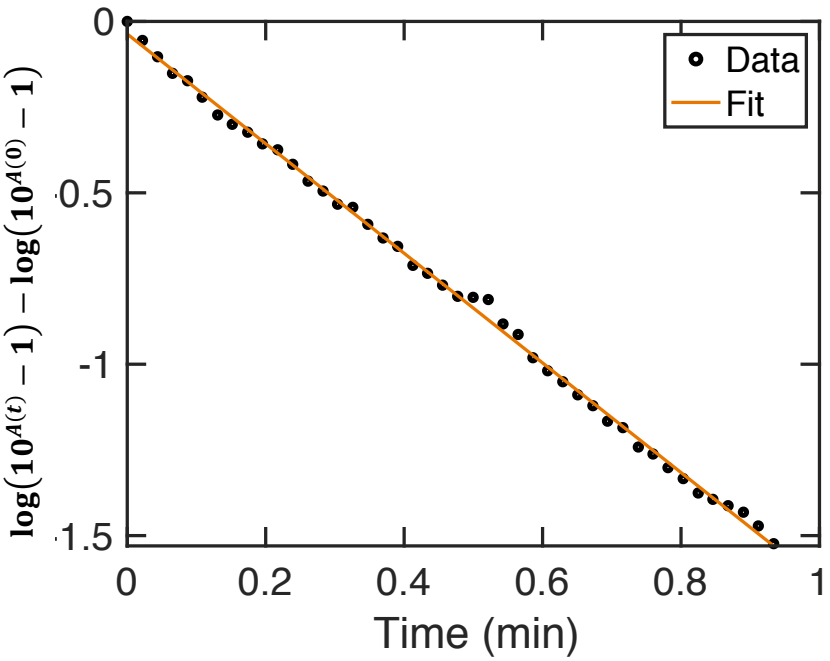

Figure S22. Linearized function of absorption vs. time used to determine the cycloreversion quantum yield of **2c**.

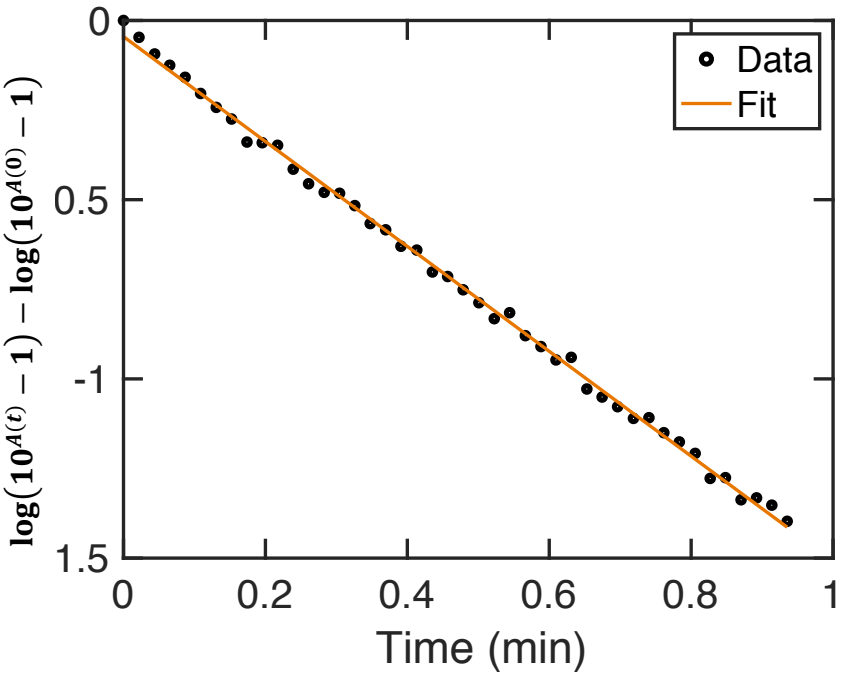

Figure S23. Linearized function of absorption vs. time used to determine the cycloreversion quantum yield of **3c**.

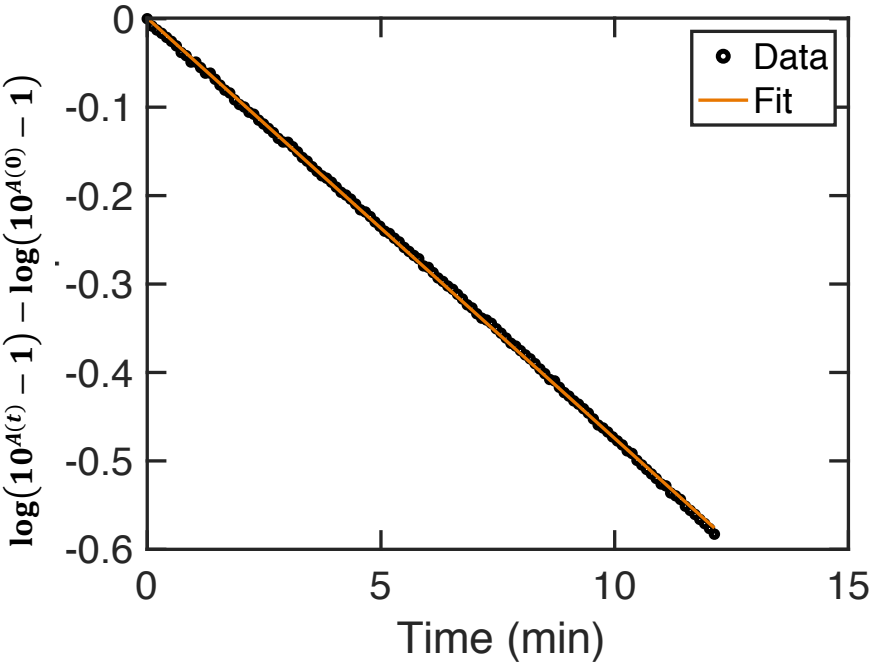

Figure S24. Linearized function of absorption vs. time used to determine the cycloreversion quantum yield of **4c**.

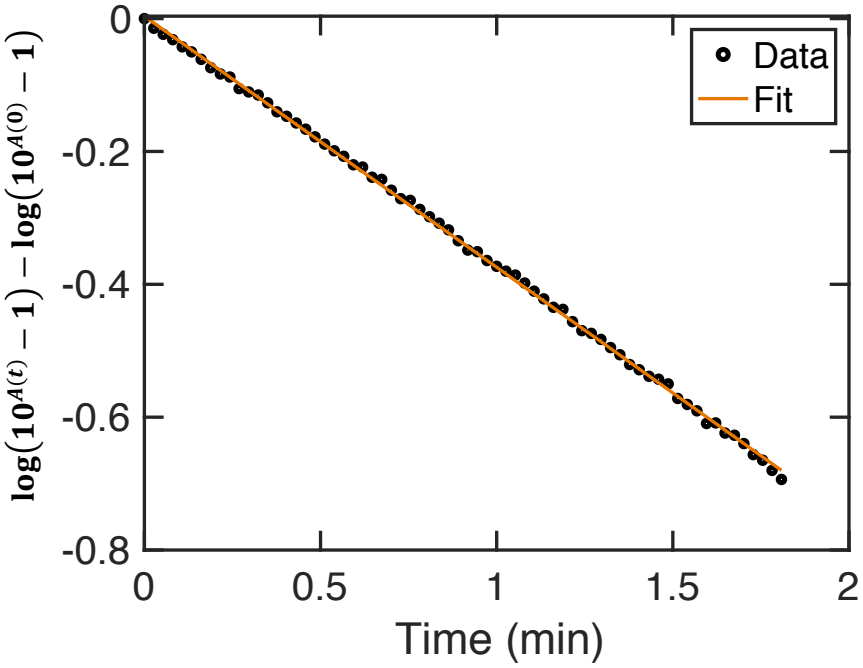

Figure S25. Linearized function of absorption vs. time used to determine the cycloreversion quantum yield of **5c**.

Table S2. Summary of results from cycloreversion quantum yield experiments for **1-5**.

Trial	1 Φ_{CO}	2 Φ_{CO}	3 Φ_{CO}	4 Φ_{CO}	5 Φ_{CO}
1	0.34	0.32	0.31	0.0046	0.11
2	0.32	0.33	0.32	0.0043	0.11
3	0.32	0.34	0.31	0.0044	0.12
4	0.31	0.36	0.32	0.0045	0.11
5	0.31	0.33	0.31	0.0041	0.12
Average	0.32	0.34	0.31	0.0044	0.12
Standard dev.	0.01	0.02	0.01	0.0002	0.002
Total propagated error	0.02	0.02	0.02	0.0003	0.006

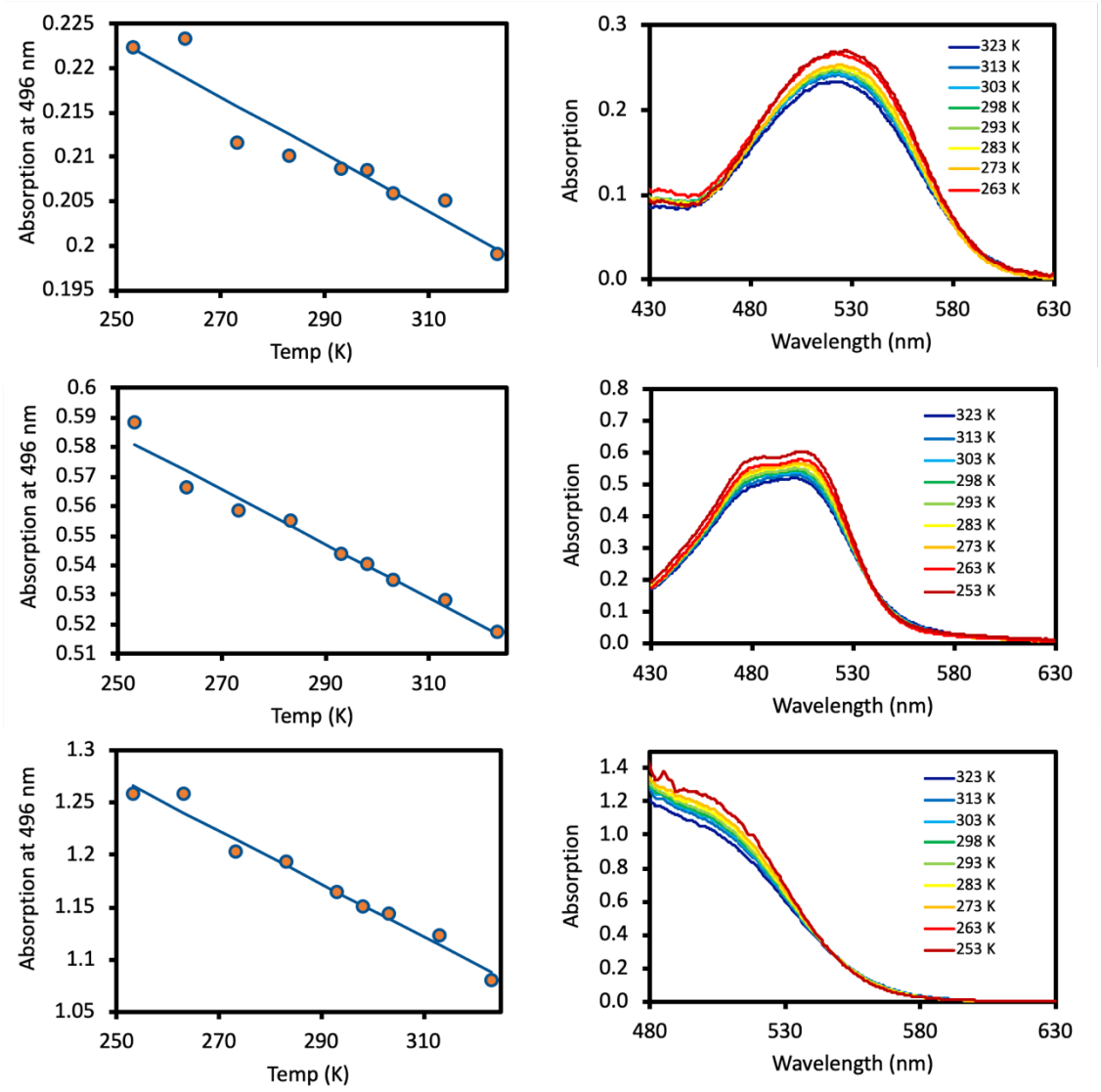

Figure S26. Temperature dependent absorption of **1c** (top), **2c** (middle), and **3c** (bottom) in acetonitrile.

Table S3. Linear egression parameters for temperature dependent molar absorptivities. The concentration of the sample was determined using the absorption data at 298K as an approximation for the absorption at room temperature.

Species	Slope (K^{-1})	Error (K^{-1})	Intercept (M^{-1} cm^{-1})	Error ($M^{-1}cm^{-1}$)
1c	-12	2	11333	436
2c	-12	1	10959	230
3c	-16	1	12058	280

Table S4. Temperature dependent changes in quantum yields for **1c**-**3c**.

Temperature (K)	1 Φ_{CO}	2 Φ_{CO}	3 Φ_{CO}
323	0.32	0.36	0.32
308	0.34	0.34	0.31
298	0.30	0.33	0.31
288	0.30	0.33	0.31
273	0.28	0.32	0.28
263	0.26	0.31	0.27
253	0.25	0.31	0.26
Slope	0.0013	0.0007	0.0009
Intercept	-0.06	0.13	0.03

5. Calculation of competitive excited-state deactivation rates and thermodynamic activation parameters.

The calculations pertaining to these properties are described in the main text in Eq. 1-6. Figures describing the activations enthalpies and entropies are shown below.

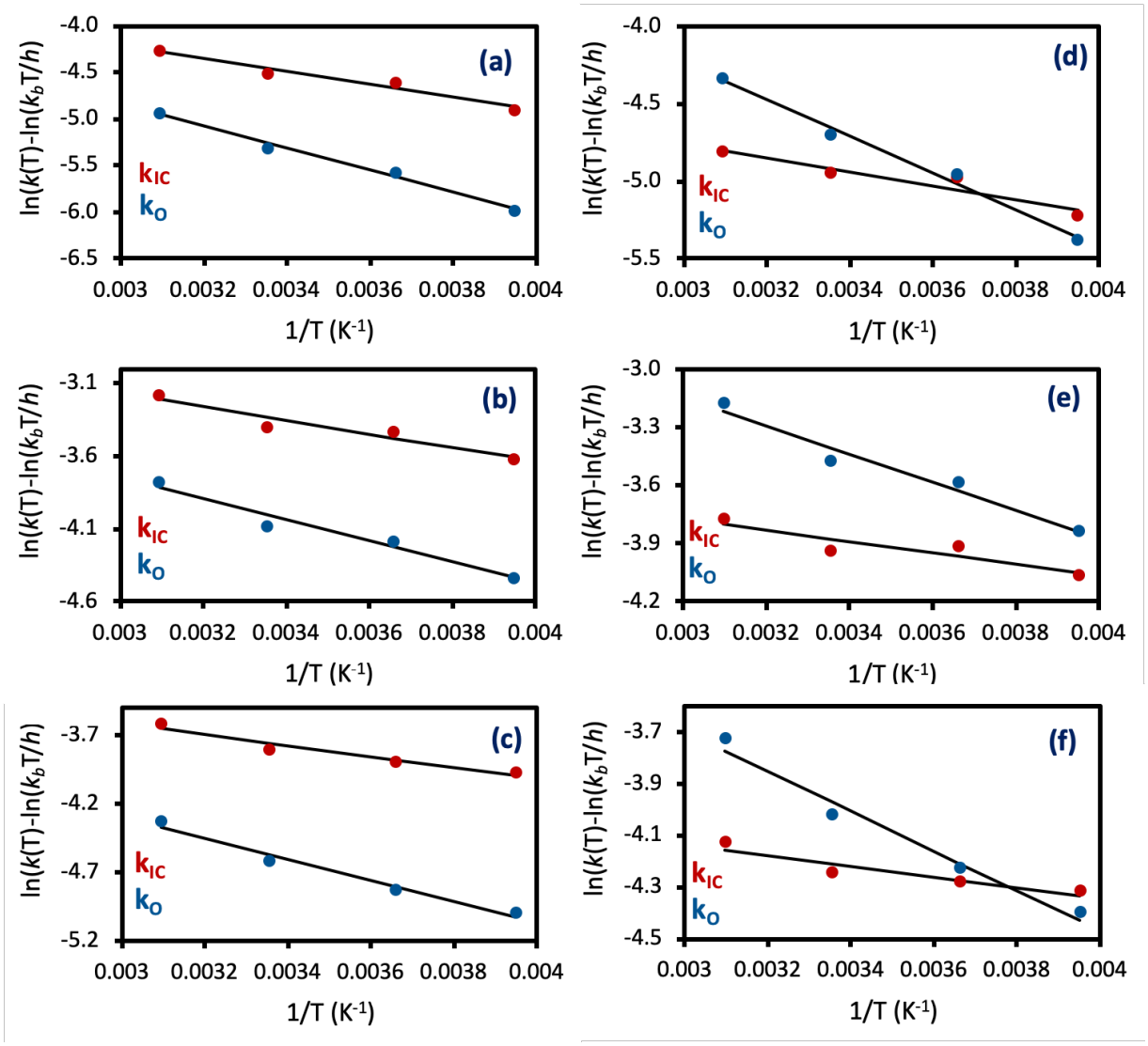

Figure S27. Plots for deriving activation enthalpies and entropies from k_{IC} and k_O for **1c-3c** assuming no branching in a, b, and c respectively, and assuming branching in d, e, and f respectively. Rates are in units of s^{-1}.

6. Spectrum of UV hand-lamp emission.

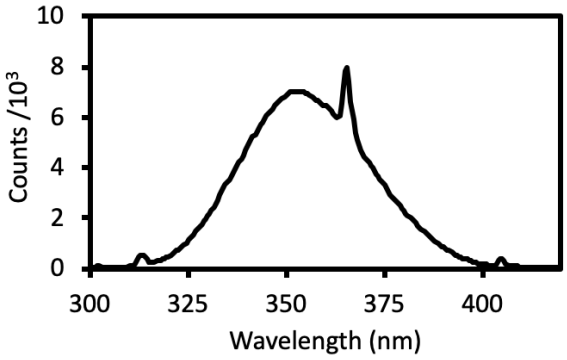

Figure S28. Spectrum of UV hand lamp used to irradiate photoswitches to achieve a photostationary state of cyclized product.